A quantitative model for oral administration of living therapeutics

Zachary JS Mays[1] and Nikhil U Nair[1]*

[1] Department of Chemical & Biological Engineering, Tufts University, Medford, MA 02155

* nikhil.nair@tufts.edu; @nair_lab

Abstract

As medicine shifts toward precision-based and personalized therapeutics, utilizing more complex biomolecules to treat increasingly difficult and rare conditions, microorganisms provide an avenue for realizing the production and processing necessary for novel drug pipelines. More so, probiotic microbes can be co-opted to deliver therapeutics by oral administration as living drugs, able to survive and safely transit the digestive tract. As living therapeutics are in their nascency, traditional pharmacokinetic-pharmacodynamic (PK-PD) models for evaluating drug candidates are not appropriate for this novel platform. Using a living therapeutic in late-stage clinical development for phenylketonuria (PKU) as a case study, we adapt traditional oral drug delivery models to properly evaluate and inform the engineering of living therapeutics. We develop the adapted for living therapeutics compartmental absorption and transit (ALT-CAT) model to provide metrics for drug efficacy across nine age groups of PKU patients and evaluate model parameters that are influenced by patient physiology, microbe selection and therapeutic production, and dosing formulations.

Importance

This work describes a kinetic model to study the behavior of orally delivered living therapeutics. Such therapeutics are becoming increasingly relevant and are an exciting mode of drug delivery that stems from the growing interest through the convergence of advances in synthetic biology of probiotics and gut microbes as well as microbiome science. In particular, this work describes the development of a mathematical framework (pharmacokinetic-pharmacodynamic, PK-PD) called ALT-CAT to model the behavior of orally delivered engineered bacteria that act as living therapeutics by adapting similar methods that have been developed and widely-used for small molecular drug delivery and absorption.

Introduction

The most common and practical route of drug delivery is oral ingestion, pairing patient convenience and high compliance with ease of administration and stability. While a simple initial assessment of a drug's biochemical feasibility for oral delivery can be predicted using the biopharmaceutical classification system (BCS) (1) or rule of five (Ro5) (2), these evaluations do not inform the further complexities of selecting lead candidates, developing a dosage or release strategy, effective bioavailability, and pharmacokinetics. Accordingly, a range of models – *in vitro* (3) and *in vivo* (4), static (5) and dynamic (6, 7), molecular (8) and system environment (9) – are used extensively in drug development to evaluate and hone desired features.

An economically appealing alternative, trading human capital and consumables for computational resources (time and power), is the modeling of drug absorption in the gastrointestinal tract (GIT). *In silico* models have been developed for both molecular interactions (10), such as receptor binding or transport, and physiology-based pharmacokinetics (PBPK) (11), such as compartment disposition or clearance. Several commercial software packages based on these models (12–14) incorporate drug physiochemical properties (solubility, degradation, permeability, molecular size, aggregation, charge), formulation properties (dosage, drug release profiles, absorption enhancers, matrix polymorphism), and GI physiological properties (gastric emptying, intestinal pH, motility, luminal content, transporters, metabolism, epithelial sequestration, disease state). Most notably, GastroPlus™ (Simulations Plus, Lancaster, CA) was conceived from the advanced compartmental absorption and transit (ACAT) model (15), separating the small intestine (SI) into a series compartments and solving the differential equations surrounding drug mass transfer.

While *in silico* oral drug absorption models have proven invaluable to the drug development pipeline, an emerging class of therapeutic candidates are not addressed with current methodologies. Living therapeutics (also termed microbiome-based therapeutics, microbial biotherapeutics, and probiotics 2.0) are engineered microorganisms that

49 have been programmed to produce drugs, potentially with autonomous contextual awareness (16–18). These
50 microbes are chosen and designed to be compatible with the human gut microbiota, acting not only as drug
51 producers but as delivery vehicles that can survive and traverse the harsh environment of the gut. The living
52 therapeutics platform offers several potential advantages including a constant or timed drug release, real-time dose
53 changes, spatial targeting of delivery, sub-clinical detectability, and the production of large or complex
54 biomacromolecules normally incompatible with oral delivery (19). The latter is the basis of an enzyme-substitution
55 therapy (EST) for phenylketonuria (PKU) in probiotic *Escherichia coli* Nissle 1917 (EcN) that is currently in Phase 1/2a
56 clinical trials (SYNB1618, Synlogic Inc; ClinicalTrials.gov identifier NCT03516487) (20). Here, the enzyme
57 phenylalanine ammonia-lyase (PAL) expressed in EcN converts excess toxic phenylalanine (phe) to the non-
58 metabolite *trans*-cinnamic acid (*t*CA) and provides therapeutic benefit.
59
60 It is clear where the limitations of current oral drug absorption models arise when considering living therapeutics.
61 The "drug" being delivered is actually a microbe that produces a catalytically active enzyme, can adhere to the gut
62 mucosal layer, can replicate, and change PAL expression levels. Furthermore, if a PKU patient consumes protein
63 containing phe, absorption of phe is counterproductive, while degradation (i.e. PAL conversion of phe to *t*CA) is the
64 desired outcome. Thus, this model must account for competition between absorption of a toxin (phe) and catalytic
65 depletion by an enzyme. Finally, just as first-pass hepatic elimination affects a drug bioavailability profile,
66 enterorecirculation of amino acids can affect concentrations of phe in the gut lumen and boost the efficacy of PAL
67 independent of meal phe (21).
68
69 Using a PAL-based treatment of PKU as the case study for living therapeutic treatments (20, 22–25), this work
70 presents the adapted for living therapeutics compartmental absorption and transit (ALT-CAT) *in silico* model, which
71 incorporates the physiology of the GI tract, different bacterial chassis, and different expression levels of PAL into the
72 traditional compartmental model (9). The CAT model was adapted to populate the SI with a microbial population

and combined with the stochastic gastric emptying (sGE) model to simulate a non-linear emptying of the stomach. A fraction of the microbial population was designated to be a living therapeutic expressing PAL to degrade phe. A therapeutic factor (TF) was created to assess model parameters such as bacteria population, enzyme activity, and phe transport. Target concentrations of phe in the blood were used as output for therapeutic efficacy. This work presents a refreshed toolset for the evaluation and comparison of living therapeutic constructs and their parts therein, serving as a benchmark for designing orally administered drug formulations.

Model construction

The original CAT model determined that a cumulative time frequency distribution of 400 human SI transit times is best represented by seven equal transit compartments (Equation 1). Drug absorption can then be derived within each compartment, relating drug bioavailability to its effective permeability coefficient (P_{eff}) (Equation 2). Drug dissolution, pH-dependent solubility, first-pass hepatic metabolism, degradation, and other region-dependent factors were added later in the ACAT model, the foundation for GastroPlus™ software. With these equations, M_n is the amount of drug in the nth compartment (mg); k_T is the transit rate constant through the compartment (min^{-1}); T_{SI} is the average transit time through the small intestine (min); r is the luminal radius (cm); and F_a is the fraction of dose absorbed (9). In our modification, we model the dynamics of toxin (phe in case of PKU) absorption using these equations.

$$\frac{dM_n}{dt} = k_T M_{n-1} - k_T M_n, \qquad n = 1, 2, \ldots, 7 \qquad \text{Equation 1}$$

$$F_a = 1 - \left(1 + \frac{2P_{eff}\langle T_{SI}\rangle}{7\mathrm{r}}\right)^{-7} \qquad \text{Equation 2}$$

While gastric and colonic drug absorption were included in the CAT model as well, the stomach is modeled by linear emptying, and flow is estimated by first-order ordinary differential equations as a plug-flow reactor (26). Physiologically, gastric emptying is a more complex process involving churning contractions, both peristalsis and retroperistalsis, controlled opening of the pyloric sphincter, solid versus liquid digesta, and hormonal feedback to

94 macronutrient composition. These coordinated movements are observed as sporadic and irregular bolus injections
95 over approximately three to four hours. Several continuous smooth equations have been employed to loosely
96 generalize observed data (27), but more recently, to better account for this, a stochastic gastric emptying (sGE)
97 model was developed by adapting the power exponential form of a standard Wiener process (Equation 3). This was
98 then used to track a decreasing monotonic jump process (Equation 4). Here, α and β are empirical parameters found
99 to give 90% confidence intervals that describe the data in Locatelli, *et al.* (2009) (28).

$$\boldsymbol{X(t) = e^{-\alpha|W(t)|^{\beta}}} \qquad \text{Equation 3}$$

$$\boldsymbol{S(t) = \min_{0<s<t} X(s)} \qquad \text{Equation 4}$$

$$\boldsymbol{\frac{dM_s}{dt} = f(S) : [\tau_{i-1}, \tau_i] \rightarrow \mathbb{R}, \qquad i = 1, 2, \ldots, T_s} \qquad \text{Equation 5}$$

100 A crucial difference between modeling traditional oral drug delivery and an EST is that the former is designed to
101 maximize absorption (and therefore bioavailability) of a drug, while the latter is meant to prevent absorption of a
102 toxic metabolite. With highly permeable or quickly transported small molecules, such as phe in the case of PKU, the
103 rate limiting step of absorption is gastric emptying. As such, modeling gastric emptying more accurately with the
104 sGE model and combining this with the ACAT model was the framework for constructing the ALT-CAT model for
105 PKU treatment (Figure 1). A spline function can be interpolated from the sGE model over the total gastric emptying
106 time (T_{GE}) to calculate instantaneous emptying rates entering the SI (Equation 5).
107

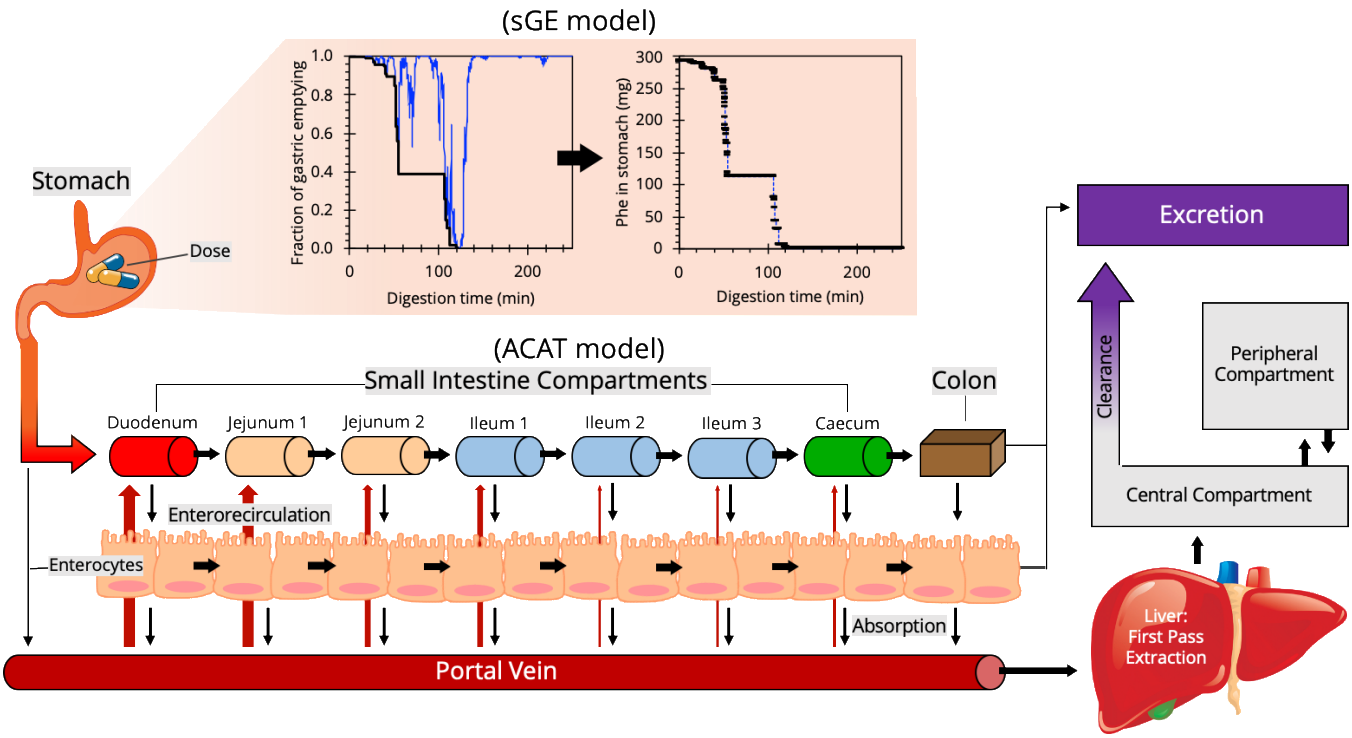

Figure 1. Schematic of the ALT-CAT model for drug absorption.
As in the ACAT model, the stomach empties into a seven compartment SI. Mass transfer differential equations surround the fate of a drug in each compartment, which ultimately defines drug bioavailability. The ALT-CAT model adapts this framework by incorporating the stochastic gastric emptying (sGE) model (orange) of the stomach and, in the case of PKU, models phe absorption as detrimental and phe degradation as therapeutic, with enterorecirculation (red arrows) contributing to luminal phe. Adapted from Agoram et al. (2001) and Macheras et al. (2003) (15, 29).

Within each compartment of the ACAT model, the instantaneous concentration of a drug transiting the gut (30) is balanced with diffusion or transport into the plasma, dissolution, degradation, aggregation, and pH-dependent solubility. While certain physiochemical or formulation properties are simplified with phe, the ALT-CAT model requires the additional mass transport of phe from the blood back into the gut lumen, a phenomenon known as amino acid enterorecirculation or exsorption. This likely occurs from both epithelial polarity (21) – active and passive transport variation between the apical (*AP*) and basolateral (*BL*) membranes of the endothelium – and pancreatic and glandular secretions during digestion (30). Transport of phe across a Caco-2 monolayer has been previously modeled as a combination of saturable and non-saturable uptake (*u*) and efflux (*e*) in both directions (Equation 6-8) (31), approximately ten times higher in the AP-to-BL direction (32). Nonlinear kinetics require phe-specific max

flux (J_{max}) (mmol mg^{-1} min^{-1}) and half maximum concentration (K_M) (mM) values, while first-order kinetics are described by phe-specific flux constants (f). Predicted plasma (p), intracellular (i), and luminal (l) phe concentrations can then inform the model, and enterorecirculation is represented as a net flux (J_{net}) ratio and incorporated in the nth compartment absorption scale factor (β_n).

$$\boldsymbol{J_{net}^{AP}} = \langle \frac{\boldsymbol{J_{max}^{u,AP} C_l}}{\boldsymbol{K_M^{u,AP} + C_l}} + \boldsymbol{f^{u,AP} C_l} \rangle - \langle \boldsymbol{f^{e,AP} C_i} \rangle \qquad \text{Equation 6}$$

$$\boldsymbol{J_{net}^{BL}} = \langle \boldsymbol{f^{e,BL} C_i} \rangle - \langle \frac{\boldsymbol{J_{max}^{u,BL} C_p}}{\boldsymbol{K_M^{u,BL} + C_p}} + \boldsymbol{f^{u,BL} C_p} \rangle \qquad \text{Equation 7}$$

$$\boldsymbol{\beta_n} = \frac{\boldsymbol{J_{net,n}^{BL}}}{\boldsymbol{J_{net,n}^{AP}}} \qquad \text{Equation 8}$$

To complete the ALT-CAT model, phe degradation can be reframed as therapeutic conversion by PAL. The GIT is populated with more than 1000 species of microorganisms in a community known as the human microbiota. This diverse population is thought to have evolved with the mammalian gut with spatial organization and niche regioselectivity determined by inextricably complex community interactions and ecological synergy. While much of the human microbiota reside in the large intestine, a low but longitudinally increasing microbial population can survive and reside in the SI. The boundaries for microbial biomass present in the duodenum, jejunum, and ileum have been reported (33), with lactic acid bacteria, a group in which the majority of probiotics are classified, encompassing approximately 0.1-10% of the population (34). Using these regional population metrics, the SI can be randomly populated with a living therapeutic population ($M_{LT,n}$) that defines nth compartment PAL delivery (Figure 2). Furthermore, phe conversion (i.e. PAL expression and activity) can be approximated across the population, with Michaelis-Menten enzyme kinetics (J_{max} and K_M) defining both phe transport (Equation 9) and PAL activity (Equation 10). These adjustments form the ALT-CAT model (Equation 11), using changes in blood plasma phe concentration (Equation 12) as a metric for therapeutic efficacy.

$$\boldsymbol{J_{tr}} = \frac{\boldsymbol{V_{max}^{tr} C_l}}{\boldsymbol{K_M^{tr} + C_l}} \qquad \text{Equation 9}$$

$$J_c = f(J_{tr}) \begin{cases} J_{tr} > J_{c,max} & \dfrac{k_{cat} C_l}{M_{LT}} \\ J_{tr} \leq J_{c,max} & \dfrac{V_{max}^{PAL} C_{i,LT}}{K_M^{PAL} + C_{i,LT}} \end{cases} \qquad \text{Equation 10}$$

$$\frac{dM_n}{dt} = k_t M_{n-1} - \beta_n k_a M_n - k_c M_n, \qquad n = 1, 2, \ldots, 7 \qquad \text{Equation 11}$$

$$\frac{dC_p}{dt} = \frac{k_a}{V} \sum_{n=1}^{7} \beta_n M_n \qquad \text{Equation 12}$$

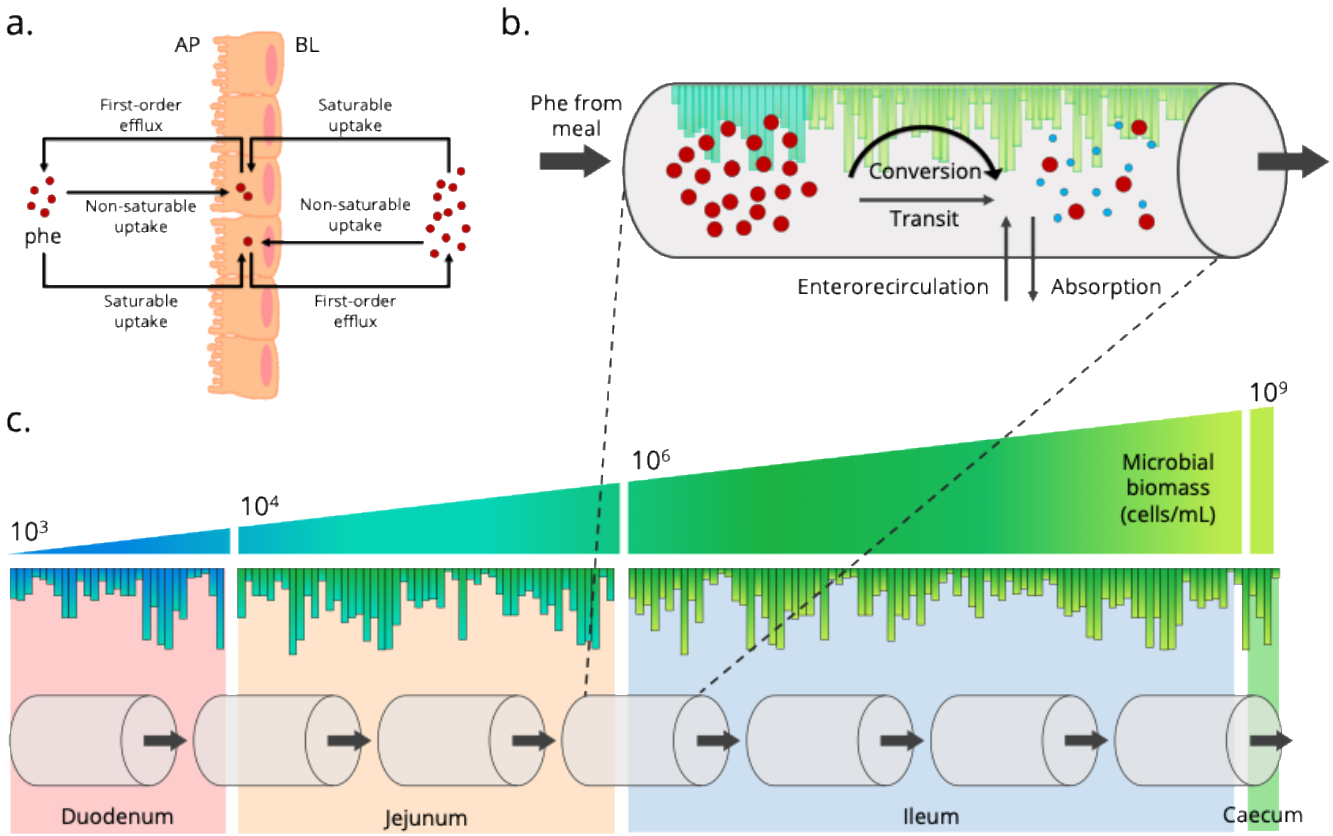

Figure 2. Populating the small intestines with living therapeutics
(a.) In PKU, enterorecirculation of phe back into the lumen contributes to (b.) the mass transfer equations driving phe degradation (therapeutic conversion) by PAL present in each compartment's living therapeutic population. (c.) Each section of the SI has a defined microbial population range. Cross-sections, similar to column plate counts in chromatography, can be generated based on gut length, each with a bounded random microbial population. The full SI can then be equally sectioned into seven compartments as in the ACAT model. Enterorecirculation adapted from Hu and Borchardt (1992) (30).

The MATLAB files for model can be found online (https://github.com/nair-lab/ALT-CAT)

Results & Discussion

Solutions to the differential equations of the ALT-CAT model can be visualized as the change in the phe in each compartment as compared to the start-of-day plasma phe. An example average adult PKU patient, eating four meals of low phe protein over the course of the day, exhibiting 0.8% living therapeutic coverage, is represented in Figure 3. As each meal empties into the SI, it creates a compartmental spike in phe the reverberates down the SI. Blood plasma phe slowly increases over the day, peaking at midnight with a 195% increase and does not follow gastric emptying, indicating the impact that enterorecirculation has on therapeutic conversion. This is similarly highlighted by the high concentration of degraded phe (i.e *t*CA) in the urine.

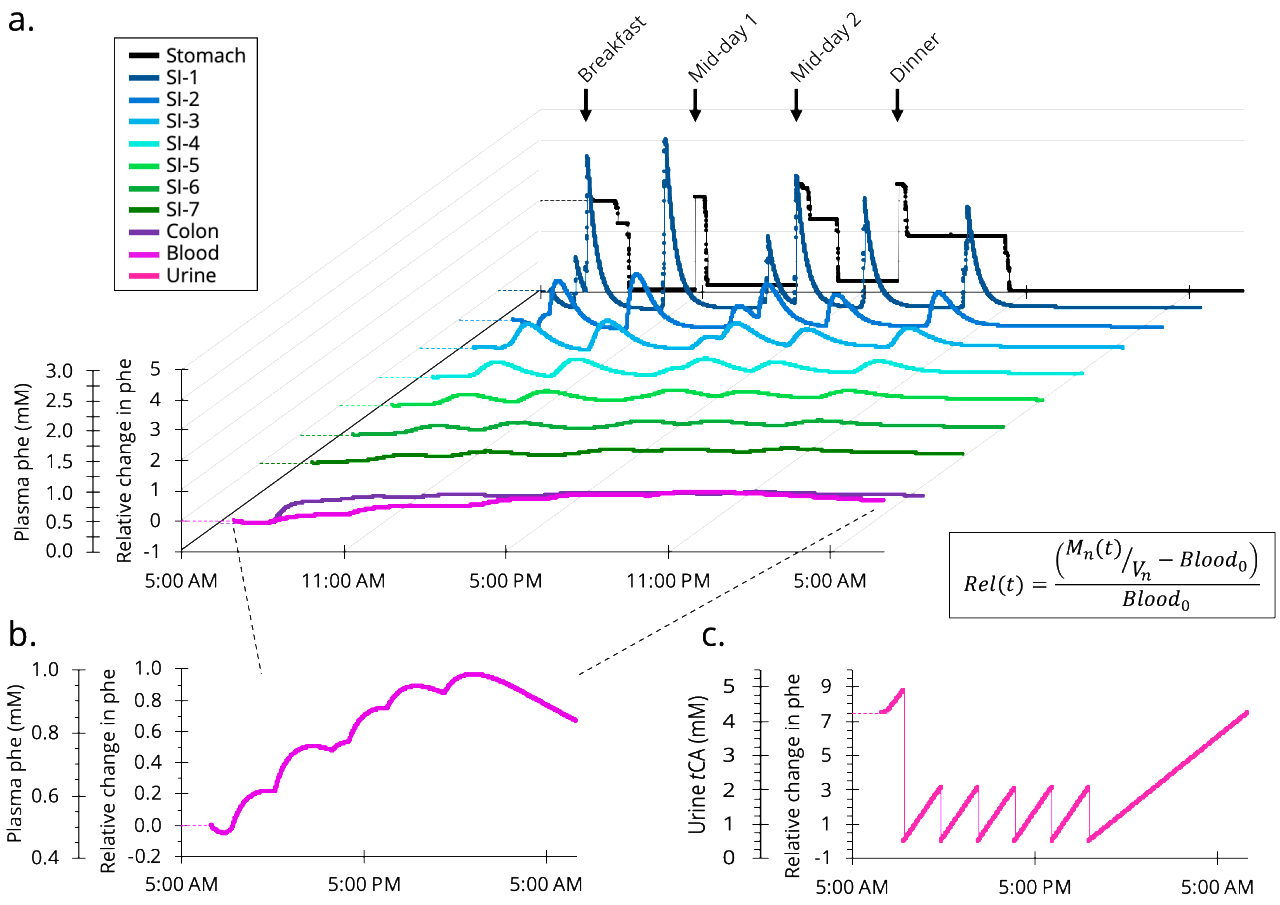

Figure 3. Representative solution to phe digestion in an adult using the ALT-CAT model.
(a.) The sGE model generates a release schedule of phe for 4 meals (average adult) over the course of 24 h. Differential equations quantify instantaneous phe in each compartment, visualized as the relative change (percent difference) in phe compared to a start-of-day plasma phe of 0.5 mM. (b.) Blood plasma phe varies by phe absorption and exsorption while a population of living therapeutic converts phe in the lumen of the seven SI compartments. (c.) Urine excretion of *t*CA, or an equivalent biomarker such as hippurate, is proportional to PAL specific activity.

167

168 Several physiological parameters of the ALT-CAT model can drastically change across a population, and thus inform,
169 the efficacy of a living therapeutic (Table 1). Drug absorption is proportional to the P_{eff}, which typically defines the
170 bioavailability of large complex drugs with poor solubility. In the case of PKU, phe is an essential amino acid that is
171 readily absorbed without much resistance, observed as sequentially less phe present in compartments of the ALT-
172 CAT model (Figure 3). Physiological properties that change between age and sex groups, such as the SI length and
173 diameter, dictate the available surface area for absorption, with villi and microvilli amplifying the cylindrical surface
174 area by 60–120 times (35). Additionally, when considering a metabolic disorder such as PKU, body size, amount of
175 protein per meal, number of meals per day, frequency of feeding, and sleep schedules can all drastically impact the
176 availability, and thus metabolism and therapeutic degradation of phe.

177

178 We ran nine age groups through the ALT-CAT model, chosen based on physiological properties of the stomach and
179 SI. Starting with a medium-high blood plasma phe concentration (0.5 mM) and 1% living therapeutic population,
180 the end-of-day concentration for 1000 simulations were observed to be influenced by these physiological factors
181 (Figure 4). Each simulation is randomly built using a normal distribution of gut length, body weight, meal phe
182 content, surface area multiplier, and microbial population (Table 1). For the infant and toddler groups, there was
183 much more variability in outcomes. Notably, an all-liquid diet at this age is better modelled as a linear gastric
184 emptying process, which, alongside a large number of meals and short intestine lengths, leave little time for
185 therapeutic conversion of phe. With the majority of phe being freely absorbed, the likely significant contributor to
186 the final distributions is the surface area multiplier (β_{SA}). Perhaps an adjuvant strategy involving phe transport
187 inhibitors would be impactful for these age groups. Large neutral amino acid (LNAA) supplementation has been
188 effective in PKU adults (36), though with the importance of amino acid concentrations for neural development, not
189 currently recommended for children. Inhibition of epithelial LNAA transporters, such as T-type amino acid
190 transporter (TAT1), with D-isomers or phe derivatives could more specifically target intestinal absorption (37, 38).

191 The ALT-CAT model reiterates reported evidence that gastric emptying is rate-limiting, and once the sGE model is
192 implemented with 7- to 12-month-olds, slower phe introduction corresponds to better therapeutic conversion (i.e.
193 lower plasma phe concentration). Older age groups have designated hours of long sleep as well, allowing phe to be
194 degraded without a meal dictating concentrations. Larger GITs obviously provide more space for more microbes as
195 a percent of the population.
196

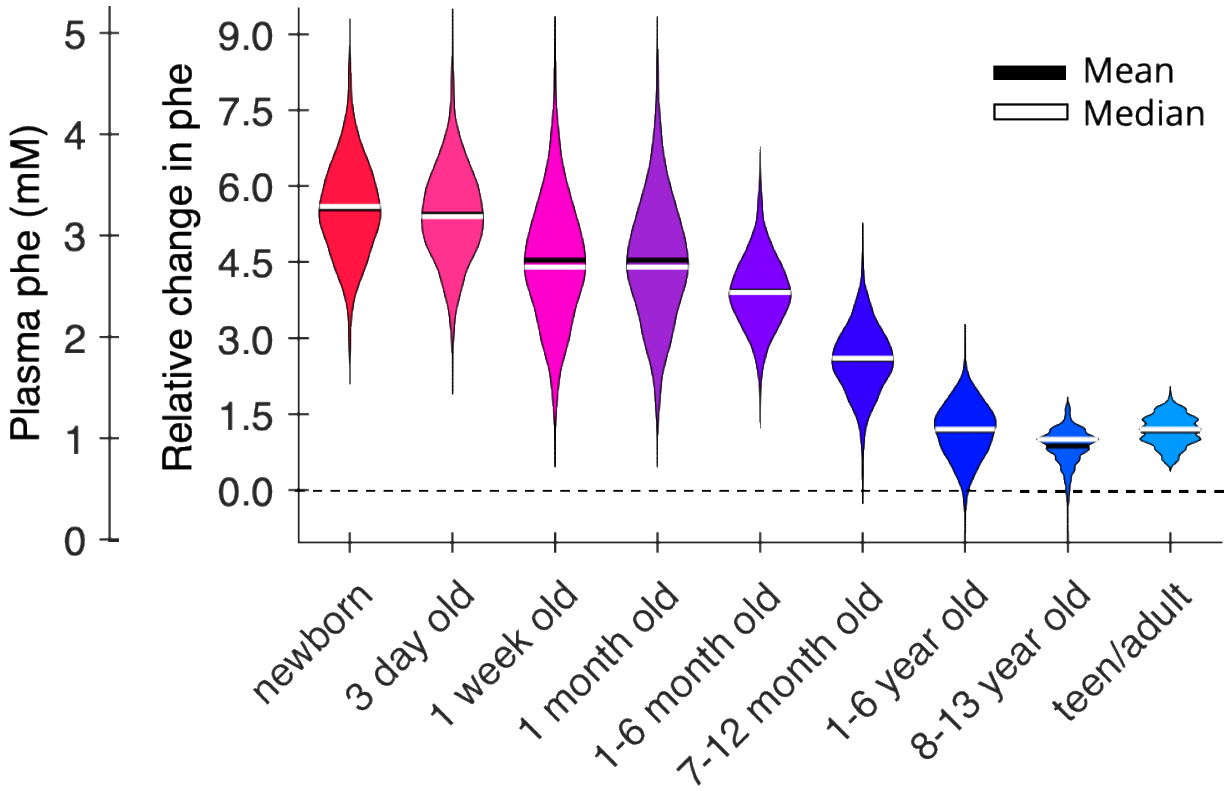

197
198 Figure 4. Changes in therapeutic efficacy across different age groups as measured by end-of-day blood phe concentration.
199 Running 1000 simulations of the ALT-CAT model across age groups in which GI physiological properties and meal sizes and
200 feeding schedules vary. The GIT is populated by designating 1% of the bacteria as the living therapeutic and results are
201 represented as a violin plot of end-of-day plasma phe concentration after a 24 h period.

202

203 Unfortunately, the physiology of the gut does not lend to metabolic intervention easily, and each age group had
204 plasma phe ubiquitously increase to unsafe levels (Figure 4). As a countering tactical measure, drug formulations for
205 living therapeutics include microencapsulation to survive the stomach (39), surface modification to improve

mucoadhesion and increase residence time or cell population (16), bacterial chassis selection to target regional success (40, 41), and enzyme choice and expression to increase specific activity per cell (40, 41). Effectively, the agenda in each case is to increase the level of therapeutic intervention at earlier stages of digestion. This can be simulated in the ALT-CAT model using a coverage multiplier (α_C) (Equation 13). This is created as the mean of a log-normal distribution to define the living therapeutic population. While it is represented as bacterial concentration in the model, this is a representative parameter of "active therapeutic agent per unit volume of SI" in each compartment, influenced by gastric survival (*G*), availability (*A*), regioselective niches (*R*), surface area (*SA*), transit time (T_{SI}), and total microbial population (M_{tot}) (Figure 5a). By increasing the α_C, the blood plasma phe concentration is noticeably impacted in both children and adults. In the 1- to 6-month-old age group, ALT-CAT model solutions with α_C = 1, which designates a mean 2.5% of the bacterial population as active, begin to lower plasma phe (Figure 5b). While this is a significant fraction of gut bacteria being replaced with the therapeutic, it corresponds to 10^{10}-10^{11} cells, within a reasonable order-of-magnitude for a dosing regimen. As the length of the SI and overall bacterial population is much larger in adults, a lower percent (α_C = 0; mean = 0.8%) is impactful. These comparisons can offer insight into dosing regimen depending on physiology, diet, and bacterial chasses.

$$\alpha_C \propto \frac{SA_{cyl}}{T_{SI}} M_{LT}(D,i,n)_{\substack{0<i<t \\ 0<n<x}} \text{ where } \left\{ \begin{array}{c} G(t) = (Dose)(gastric\ survival) \\ A(G,t) = (G_i)(dose\ release\ schedule) \\ R(A,t,x) = (A_i)(regioselective\ survival) \\ SA_{cyl} = 2\pi r_n^2 + (2\pi r_n)dx \\ M_{tot} = \dfrac{microbe\ population_n}{SA_{cyl,n}} \\ M_{LT} = \dfrac{R_{i,n}}{M_{tot,n}} \end{array} \right\} \quad \text{Equation 13}$$

$$\alpha_E \propto (J_c)(M_{LT})(E) \quad \text{Equation 14}$$

$$\alpha_T \propto \left((\beta_{SA} SA_{cyl})(\beta_n)(F_a)\right)^{-1} \quad \text{Equation 15}$$

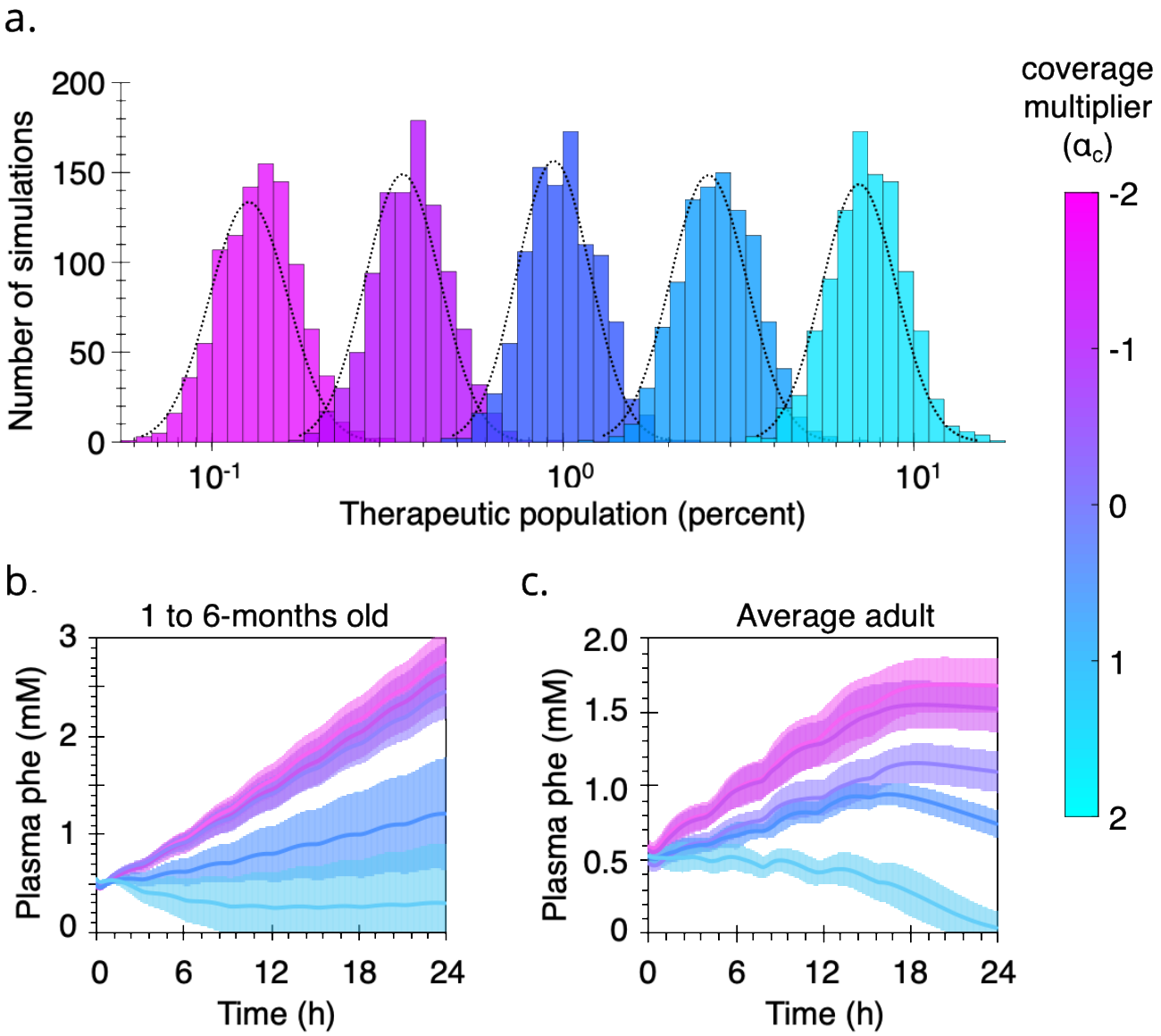

Figure 5. Therapeutic factor impacts on ALT-CAT solutions
A PAL-based living therapeutic to treat PKU is highly impacted by the number of bacteria able to degrade phe. (a.) The mean of a lognormal distribution is used to randomly populate the gut within a population range and is represented in the ALT-CAT model as the coverage multiplier (α_C). Varying α_C in the GIT of (b.) 1 to 6-month old babies and (c.) average adults, represented as the blood plasma phe concentration over a 24 h period as mean (line) and standard deviation (shaded region) of 1000 solutions.

As a thought experiment, it is more realistic to control enzyme properties within a bacterial cell than it is to control the many complex environmental interactions bacteria may encounter in the SI. Enzymatic specific activity, whether

232 that be from increased M_{LT} or higher protein expression (E) or turnover (k_{cat}), can be more informative as a metric in
233 the ALT-CAT model solution space. Thus, similar simulations with each age group were performed using an enzyme
234 multiplier (α_E) (Equation 14) applied to PAL rather than microbial population (α_C). Initially, moving from α_C = 0
235 (~0.8% cells) to α_C = 1 (~2.5% cells) yielded a bacterial population that was efficacious in 1- to 6-month-old babies;
236 this is 3.125-fold change. Reframing this, keeping the bacterial population constant but increasing specific enzyme
237 activity by 3.125-fold (i.e. α_E = 3.125) has an equivalent impact on lowering the end-of-day plasma phe (Figure 6a).
238 That is, enzyme specific activity is proportional to M_{LT}.
239

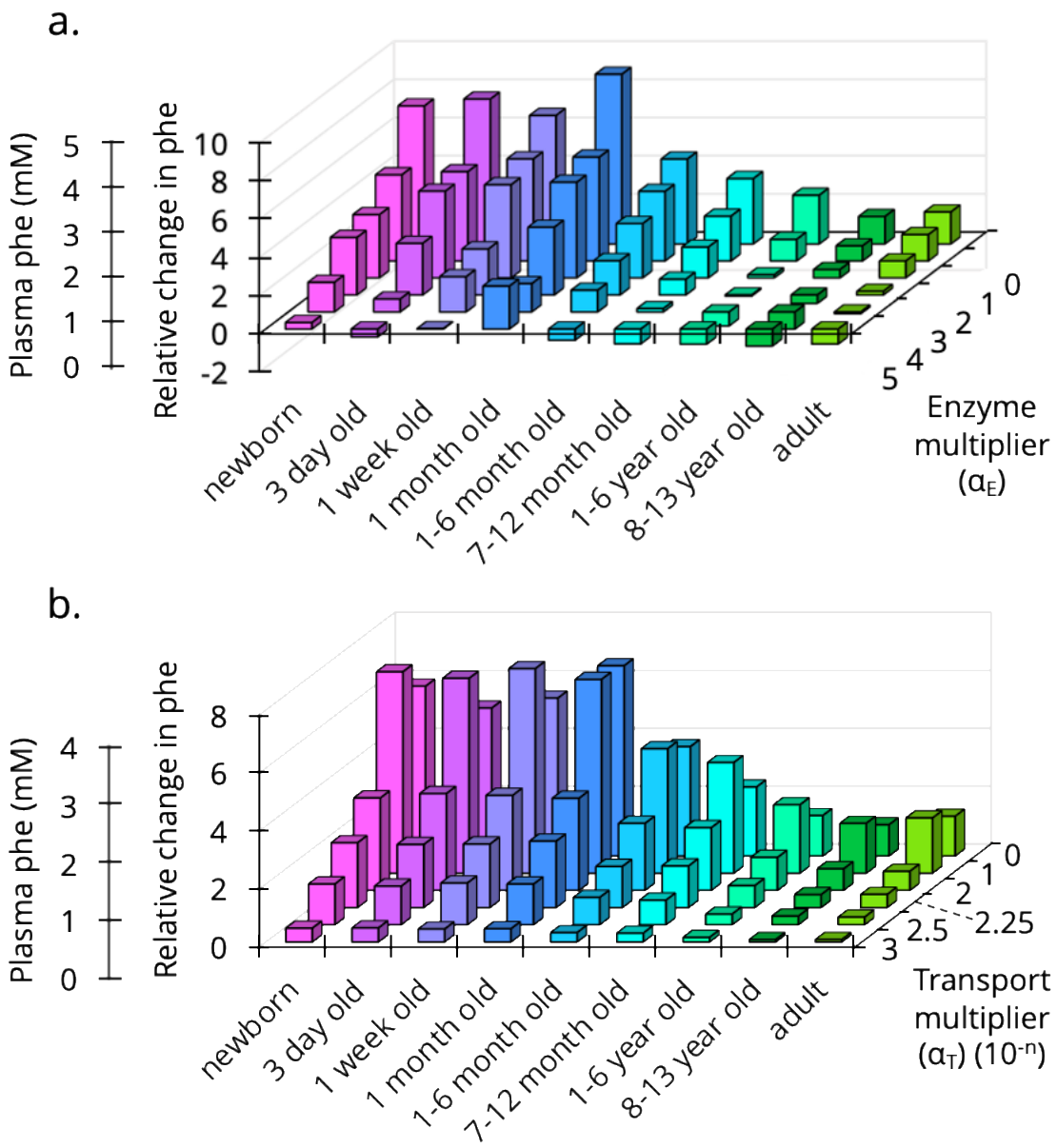

Figure 6. Exploring the solution space of the ALT-CAT model.
While keeping the coverage multiplier constant (α_C = 0; ~0.8%), the end-of-day plasma phe concentration was calculated for (a.) increasing PAL specific activity by changing the enzyme multiplier (α_E), and (b.) slowing the absorption of phe by increasing the permeability multiplier (α_T). Each bar is the mean of 100 simulations.

Alternatively, transport of phe across the epithelium is fast, approximately 4.1 × 10^{-4} cm/s (42), and on the high end of typical drugs (42, 43). Slowing P_{eff} or reducing β_{SA} or enterorecirculation (β_n) using a transport multiplier (α_T) can offer insight into the weight that transport phenomena impact drug bioavailability (or in the case of PKU, phe

absorption) from a living therapeutic (Figure 6b). Lowering the P_{eff} of phe by 225-fold (α_T = 2.25), improves the treatment 2.3-fold for 1- to 6-month-old babies (Figure 6b). This level of change unlikely to be feasible for the treatment of PKU using LNAA supplementation. However, generalizing beyond phe and treating PKU, this new P_{eff} ~10^{-4} to 10^{-5} cm/s (i.e. α_T = 2.25) falls within the range of typical small molecule drugs (42, 43). So, considering these trends conceptually as the production of a typical drug with a living therapeutic, if the drug has poor bioavailability (α_T = 0), the current-best-reported production (α_E = 1) would require ~2.5% population coverage (α_C = 1). However, improving drug bioavailability by increasing permeability (α_T = 2.25) now only requires ~1% (or 2.5 ÷ 2.3) of the bacterial population to produce the same efficacy, or approximately α_C = 0. Slower absorption requires a lower dose. These model adjustments provide examples as to how tuning different parameters can inform design benchmarks when constructing living therapeutics for different applications.

These three parameters (bacterial population, enzyme activity, and transport) represent avenues of engineering. As such, a combinatorial approach to dial in system- or therapy-specific parameters can be informed by running the ALT-CAT model to set investigative benchmarks and clinical boundaries. Additional drug physiochemical and formulation properties and GI physiological properties can easily be added and assessed using multipliers as explored in Figure 6. While PKU and a PAL-based EST offer a well-suited case study for the development and evaluation of the ALT-CAT model, we present this as a generalized tool for oral drug development and the advancement of living therapeutics as a platform.

Supplemental Information

The MATLAB files for model can be found at the Nair lab GitHub page: https://github.com/nair-lab/ALT-CAT

Funding

This work was financially supported by grant numbers R03HD090444 and DP2HD091798 of the National Institutes of Health.

Conflict of Interest

None.

References

1. Amidon GL, Lennernäs H, Shah VP, Crison JR. 1995. A Theoretical Basis for a Biopharmaceutic Drug Classification: The Correlation of in Vitro Drug Product Dissolution and in Vivo Bioavailability. Pharmaceutical Research: An Official Journal of the American Association of Pharmaceutical Scientists 12:413–420.
2. Lipinski CA, Lombardo F, Dominy BW, Feeney PJ. 2012. Experimental and computational approaches to estimate solubility and permeability in drug discovery and development settings. Advanced Drug Delivery Reviews 64:4–17.
3. Turco L, Catone T, Caloni F, Consiglio E di, Testai E, Stammati A. 2011. Caco-2/TC7 cell line characterization for intestinal absorption: How reliable is this in vitro model for the prediction of the oral dose fraction absorbed in human? Toxicology in Vitro 25:13–20.
4. Lennernäs H, Ahrenstedt Ö, Hällgren R, Knutson L, Ryde M, Paalzow LK. 1992. Regional Jejunal Perfusion, a New in Vivo Approach to Study Oral Drug Absorption in Man. Pharmaceutical Research: An Official Journal of the American Association of Pharmaceutical Scientists.
5. Antunes F, Andrade F, Araújo F, Ferreira D, Sarmento B. 2013. Establishment of a triple co-culture in vitro cell models to study intestinal absorption of peptide drugs. European Journal of Pharmaceutics and Biopharmaceutics 83:427–435.
6. Bein A, Shin W, Jalili-firoozinezhad S, Park MH, Kim HJ, Ingber DE. 2018. Microfluidic Organ-on-a-Chip Models of Human Intestine. Cellular and Molecular Gastroenterology and Hepatology 5:659–668.
7. Minekus M, Smeets-Peeters M, Havenaar R, Bernalier A, Fonty G, Marol-Bonnin S, Alric M, Marteau P, Huis In't Veld JHJ. 1999. A computer-controlled system to simulate conditions of the large intestine with peristaltic mixing, water absorption and absorption of fermentation products. Applied Microbiology and Biotechnology 53:108–114.
8. Basant N, Gupta S, Singh KP. 2016. Predicting human intestinal absorption of diverse chemicals using ensemble learning based QSAR modeling approaches. Computational Biology and Chemistry 61:178–196.
9. Yu LX, Amidon GL. 1999. A compartmental absorption and transit model for estimating oral drug absorption. International Journal of Pharmaceutics 186:119–125.
10. di Meo F, Fabre G, Berka K, Ossman T, Chantemargue B, Paloncýová M, Marquet P, Otyepka M, Trouillas P. 2016. In silico pharmacology: Drug membrane partitioning and crossing. Pharmacological Research 111:471–486.
11. Rowland M, Peck C, Tucker G. 2011. Physiologically-Based Pharmacokinetics in Drug Development and Regulatory Science. Annual Review of Pharmacology and Toxicology 51:45–73.

309 12. Willmann S, Thelen K, Lippert J. 2012. Integration of dissolution into physiologically-based pharmacokinetic
310 models III: PK-Sim. Journal of Pharmacy and Pharmacology 64:997–1007.
311 13. Marsousi N, Desmeules JA, Rudaz S, Daali Y. 2018. Prediction of drug-drug interactions using physiologically-
312 based pharmacokinetic models of CYP450 modulators included in Simcyp software. Biopharmaceutics and
313 Drug Disposition 39:3–17.
314 14. Gobeau N, Stringer R, de Buck S, Tuntland T, Faller B. 2016. Evaluation of the GastroPlus™ Advanced
315 Compartmental and Transit (ACAT) Model in Early Discovery. Pharmaceutical Research 33:2126–2139.
316 15. Agoram B, Woltosz WS, Bolger MB. 2001. Predicting the impact of physiological and biochemical processes on
317 oral drug bioavailability. Advanced Drug Delivery Reviews 50:S41–S67.
318 16. Mays ZJ, Nair NU. 2018. Synthetic biology in probiotic lactic acid bacteria: At the frontier of living therapeutics.
319 Curr Op Biotechnol 53:224–231.
320 17. Bober JR, Beisel CL, Nair NU. 2018. Synthetic Biology Approaches to Engineer Probiotics and Members of the
321 Human Microbiota for Biomedical Applications 277–300.
322 18. Waller MC, Bober JR, Nair NU, Beisel CL. 2017. Toward a genetic tool development pipeline for host-associated
323 bacteria. Curr Opin Microbiol 38:156–164.
324 19. Mimee M, Citorik RJ, Lu TK. 2016. Microbiome therapeutics — Advances and challenges. Advanced Drug
325 Delivery Reviews 105:44–54.
326 20. Isabella VM, Ha BN, Castillo MJ, Lubkowicz DJ, Rowe SE, Millet YA, Anderson CL, Li N, Fisher AB, West KA, Reeder
327 PJ, Momin MM, Bergeron CG, Guilmain SE, Miller PF, Kurtz CB, Falb D. 2018. Development of a synthetic live
328 bacterial therapeutic for the human metabolic disease phenylketonuria. Nat Biotechnol 36:857–867.
329 21. Chang S, Ming T, Bourget L, Lister C. 1995. A new theory of enterorecirculation of amino acids and its use for
330 depleting unwanted amino acids using oral enzyme-artificial cells, as in removing phenylalanine in
331 phenylketonuria. Artificial Cells, Blood Substitutes, and Biotechnology 23:1–21.
332 22. West KA, Perreault M, Kurtz CB, Wagner DA, Charbonneau MR, Dagon Y, Degar AJ, Kotula JW, Millet YA,
333 Brennan AM, Miller PF, Puurunen MK, Denney WS, Isabella VM, Antipov E. 2019. An engineered E. coli Nissle
334 improves hyperammonemia and survival in mice and shows dose-dependent exposure in healthy humans. Sci
335 Transl Med 11:eaau7975.
336 23. Rhimi M, Bermudez-Humaran LG, Huang Y, Boudebbouze S, Gaci N, Garnier A, Gratadoux JJ, Mkaouar H,
337 Langella P, Maguin E. 2015. The secreted l-arabinose isomerase displays anti-hyperglycemic effects in mice.
338 Microbial Cell Factories 14:204.
339 24. Lin Y, Krogh-Andersen K, Hammarström L, Marcotte H. 2017. Lactobacillus delivery of bioactive interleukin-22.
340 Microbial Cell Factories 16:148.
341 25. Zhang B, Li A, Zuo F, Yu R, Zeng Z, Ma H, Chen S. 2016. Recombinant Lactococcus lactis NZ9000 secretes a
342 bioactive kisspeptin that inhibits proliferation and migration of human colon carcinoma HT-29 cells. Microbial
343 Cell Factories 15:102.
344 26. Yu LX, Crison JR, Amidon GL. 1996. Compartmental transit and dispersion model analysis of small intestinal
345 transit flow in humans. Int J Pharm 140:111–118.
346 27. Yokrattanasak J, de Gaetano A, Panunzi S, Satiracoo P, Lawton WM, Lenbury Y. 2016. A simple, realistic
347 stochastic model of gastric emptying. PLoS ONE 11:1–15.
348 28. Locatelli I, Mrhar A, Bogataj M. 2009. Gastric emptying of pellets under fasting conditions: A mathematical
349 model. Pharmaceutical Research 26:1607–1617.
350 29. Macheras P, Karalis V, Valsami G. 2013. Keeping a critical eye on the science and the regulation of oral drug
351 absorption: A review. Journal of Pharmaceutical Sciences 102:3018–3036.
352 30. Hu M, Borchardt RT. 1992. Transport of a large neutral amino acid in a human intestinal epithelial cell line
353 (Caco-2): uptake and efflux of phenylalanine. BBA - Molecular Cell Research 1135:233–244.

354 31. Hidalgo IJ, Borchardt RT. 1990. Transport of a large neutral amino acid (phenylalanine) in a human intestinal
355 epithelial cell line: Caco-2. BBA - Biomembranes 1028:25–30.
356 32. Walter J, Ley R. 2011. The Human Gut Microbiome: Ecology and Recent Evolutionary Changes. Annu Rev
357 Microbiol 65:411–429.
358 33. Douillard FP, de Vos WM. 2014. Functional genomics of lactic acid bacteria: From food to health. Microb Cell
359 Fact 13:S8.
360 34. Helander HF, Fändriks L. 2014. Surface area of the digestive tract-revisited. Scandinavian Journal of
361 Gastroenterology 49:681–689.
362 35. Zhang Y, Jia X, Wang L, Liu J, Ma G. 2011. Preparation of Ca-alginate microparticles and its application for
363 phenylketonuria oral therapy. Industrial and Engineering Chemistry Research 50:4106–4112.
364 36. Matalon R, Michals-Matalon K, Bhatia G, Burlina AB, Burlina AP, Braga C, Fiori L, Giovannini M, Grechanina E,
365 Novikov P, Grady J, Tyring SK, Guttler F. 2007. Double blind placebo control trial of large neutral amino acids
366 in treatment of PKU: Effect on blood phenylalanine. Journal of Inherited Metabolic Disease 30:153–158.
367 37. Mariotta L, Ramadan T, Singer D, Guetg A, Herzog B, Stoeger C, Palacín M, Lahoutte T, Camargo SMR, Verrey
368 F. 2012. T-type amino acid transporter TAT1 (Slc16a10) is essential for extracellular aromatic amino acid
369 homeostasis control. Journal of Physiology 590:6413–6424.
370 38. Kim DK, Kanai Y, Chairoungdua A, Matsuo H, Cha SH, Endou H. 2001. Expression Cloning of a Na+-independent
371 Aromatic Amino Acid Transporter with Structural Similarity to H+/Monocarboxylate Transporters. Journal of
372 Biological Chemistry 276:17221–17228.
373 39. Mays ZJS, Chappell TC, Nair NU. 2020. Quantifying and Engineering Mucus Adhesion of Probiotics. ACS
374 Synthetic Biology acssynbio.9b00356.
375 40. Jendresen CB, Stahlhut SG, Li M, Gaspar P, Siedler S, Förster J, Maury J, Borodina I, Nielsen AT. 2015. Highly
376 active and specific tyrosine ammonia-lyases from diverse origins enable enhanced production of aromatic
377 compounds in bacteria and Saccharomyces cerevisiae. Applied and Environmental Microbiology 81:4458–4476.
378 41. Wu B, Szymański W, Heberling MM, Feringa BL, Janssen DB. 2011. Aminomutases: Mechanistic diversity,
379 biotechnological applications and future perspectives. Trends in Biotechnology 29:352–362.
380 42. Dahlgren D, Roos C, Sjögren E, Lennernäs H. 2015. Direct in Vivo Human Intestinal Permeability (Peff)
381 Determined with Different Clinical Perfusion and Intubation Methods. Journal of Pharmaceutical Sciences
382 104:2702–2726.
383 43. Wolk O, Markovic M, Porat D, Fine-Shamir N, Zur M, Beig A, Dahan A. 2019. Segmental-Dependent Intestinal
384 Drug Permeability: Development and Model Validation of In Silico Predictions Guided by In Vivo Permeability
385 Values. Journal of Pharmaceutical Sciences 108:316–325.

386

Table 1. Parameters entered into the ALT-CAT model

Model parameter			Value
excretion rate, k_{excr}	(min^{-1})		0.045
blood volume to weight ratio	(L kg^{-1})		0.075
enzyme to cell weight ratio	(mg mg^{-1})		0.165
effective permeability coefficient, P_{eff}	(cm min^{-1})		0.03
surface area multiplier, β_{SA}			60 to 120
maximum rate apical uptake, $J_{max}^{u,AP}$	(nmol min^{-1} mg^{-1})		16.1
phe at half max apical uptake, $K_M^{u,AP}$	(mM)		2.7
apical uptake rate constant, $f^{u,AP}$	(nmol min^{-1} mg^{-1} mM^{-1})		0.2
apical efflux rate constant, $f^{e,AP}$	(nmol min^{-1} mg^{-1} mM^{-1})		0.289
		Duodenum	10^3 to 10^4
microbe population boundaries	(cells mL^{-1})	Jejunum	10^4 to 10^6
		Ileum	10^6 to 10^9

Model parameter		Value
PAL specific activity, J_{enz}		3.5
maximum internal to luminal phe, J_{max}^{ci}	(mM)	13.26
phe at half max internal to luminal phe, K_M^{ci}	(mM)	4.203
maximum rate *E. coli* phe transport, J_{max}^{tr}	(mmol 30 s^{-1} mg^{-1})	0.75
phe at half max *E.coli* transport, K_M^{tr}	(mM)	0.00072
maximum rate basolateral uptake, $J_{max}^{u,BL}$	(nmol min^{-1} mg^{-1})	1.07
phe at half max basolateral uptake, $K_M^{u,BL}$	(mM)	0.18
basolateral uptake rate constant, $f^{u,BL}$	(nmol min^{-1} mg^{-1} mM^{-1})	0.2
basolateral efflux rate constant, $f^{e,BL}$	(nmol min^{-1} mg^{-1} mM^{-1})	0.476
sGE model alpha, α		1.00E-06
sGE model beta, β		6

Model parameter		Value								
		newborn	3-day-old	1-week-old	1-month-old	1- to 6-month-old	7- to 12-month-old	1- to 6-year-old	8- to 13-year-old	adult
SI length	(cm)	246.5 ± 56.2	246.5 ± 56.2	246.5 ± 56.2	246.5 ± 56.2	351.4 ± 97.8	359.5 ± 75.7	423.0 ± 99.0	464.2 ± 103.1	595.5 ± 101.8
SI internal diameter	(cm)	1.5	1.5	1.5	1.5	1.5	1.5	2.0	2.5	2.5
weight	(kg)	3.4 ± 0.2	3.4 ± 0.3	3.6 ± 0.2	4.4 ± 0.3	6.2 ± 0.3	7.9 ± 0.4	17.5 ± 1.7	35 ± 5.0	71.0 ± 5.1
number of meals		12	12	10	8	8	6	5	4	4
low phe diet	(mg kg^{-1} d^{-1})	58 ± 18	58 ± 18	58 ± 18	58 ± 18	40 ± 10	31 ± 8.5	20 ± 1	14 ± 1	14 ± 1
gastric half emptying time, T_{GE}	(min)	35	35	35	48	60	90	90	90	120
SI transit time, T_{SI}	(min)	1.5	1.5	1.5	1.5	3.5	3.5	3.5	3.5	3.5
sleep time	(h)	0	0	0	0	0	10	11	11	9